Artificial photosynthetic systems: assemblies of slipped cofacial porphyrins and phthalocyanines showing strong electronic coupling

Akiharu Satake and Yoshiaki Kobuke*

Received 6th March 2007
First published as an Advance Article on the web 27th April 2007
DOI: 10.1039/b703405a

This paper reviews selected types of structurally well defined assemblies of porphyrins and phthalocyanines with strong electronic coupling. Face-to-face, head-to-tail, slipped cofacial, and non-parallel dimeric motifs constructed by covalent and non-covalent bonds are compared in the earlier sections. Their molecular orientation, electronic overlap, and absorption and fluorescence properties are discussed with a view towards the development of artificial photosynthetic systems and molecular electronics. Complementary coordination dimers are fully satisfactory in terms of structural stability, orientation factor, π-electronic overlap, and zero fluorescence quenching. In later sections, several polymeric and macrocyclic porphyrin assemblies constructed by a combination of covalent bonds and complementary coordination bonds are discussed from the viewpoint of light-harvesting antenna functions.

1. Introduction

Recent studies on photosynthetic systems using X-ray crystallography,[1] cryomicroscopy[2] and AFM measurements[3] have provided clear molecular images of how solar energy is harvested to initiate photo-induced oxidation–reduction reactions. One excellent example is seen in the AFM picture of the superstructure of the photosynthetic bacterium, *Rhodospirillum photometricum*, shown in Fig. 1.[3a] This has an arrangement that is composed of complete sets for bacterial photosynthesis: light-harvesting complexes I (LH1) and II (LH2), and a reaction centre. Using crystal structures resolved at the atomic level that have been elucidated for photosynthetic units, we can design molecular systems in which light energy is captured from dilute sources and the singlet excitation energy is transferred to a final acceptor passing through a long pathway without any dissipation in energy. This type of antenna structure is most intriguing, especially from the point of view that bacteriochlorophylls are arranged into regular forms that are associated with strong electronic coupling. A similar uniform arrangement of chromophores[4] is observed in chlorosome systems. Cyanobacteria[5] and chloroplasts[6] provide different examples of chromophoric arrangements. We can learn much from the former case, since the regular arrangements of chromophores with strong electronic coupling in a well-defined

Graduate School of Materials Science, Nara Institute of Science and Technology (NAIST), Takayama 8916-5, Ikoma, Nara, 630-0192, Japan. E-mail: satake@ms.nasit.jp, kobuke@ms.naist.jp; Fax: +81-743-72-6119

Akiharu Satake received his PhD degree from Waseda University in 1995 working with Professor Isao Shimizu and Professor Akio Yamamoto. After two years with Professor Shimizu as an Assistant Professor at Waseda University, he joined the group of Dr Tadashi Nakata in RIKEN as a Special Postdoctoral Researcher in 1997. In 1999, he joined the group of Prof. Yoshiaki Kobuke in the Graduate School of Materials Science, Nara Institute of Science and Technology as an Assistant Professor.

Akiharu Satake

Yoshiaki Kobuke

Yoshiaki Kobuke received his PhD degree in 1970 from the Faculty of Engineering, Kyoto University, where he worked successively with Profs. Junji Furukawa, Iwao Tabushi and Hisanobu Ogoshi as Assistant and Associate Professors. In 1972–1973, he worked with Professor Robert Burns Woodward, Harvard University. In 1990, he was promoted to Professor at Shizuoka University. In 1998, he moved to the Graduate School of Materials Science, Nara Institute of Science and Technology.

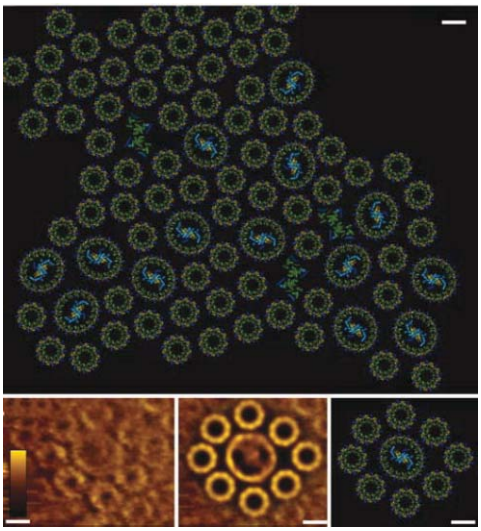

Fig. 1 Molecular organization of a photosynthetic apparatus. (Reprinted with permission from ref. 3*a*. Copyright (2004) The National Academy of Sciences, U.S.A.)

orientation must be the governing principle, on which we reliably construct artificial systems.

Well-designed molecular assemblies can produce new functions that are not observed in the corresponding monomer, and changes in the UV–vis absorption spectra from excitonic coupling,[7] efficient energy transfer,[8] photo-induced electron transfer,[9] charge transport,[10] and non-linear optics[11] are of particular interest. It is our aim to extract construction principles for assembling close-lying π-electronic systems with strong electronic coupling and no fluorescence quenching. These molecular assemblies could be used as materials for excited energy transport and electron–hole transport systems.

In this article, we review several covalent and non-covalent organizations that are composed of porphyrins and phthalocyanines. We have focused on slipped cofacial porphyrin and phthalocyanine dimers. Their molecular orientation, electronic overlap, and absorption and fluorescence properties are discussed with a view towards the development of artificial antenna systems and molecular electronics.

2. Methodologies used to construct dimers and larger aggregates

The construction of dimers that have a strong electronic interaction is the first step needed to obtain larger assemblies, and various covalent and non-covalent approaches have been reported so far.[12] Face-to-face and slipped cofacial dimers linked by alkyl chains have been synthesized using porphyrin molecules.[13] Although covalent linkages are the most reliable method used to connect two chromophores, the controlled placement of a molecule in an exact orientation is not an easy task. As reported by Hunter and Sanders,[14] the electrostatic repulsion between two π-conjugated molecules located near to one another tends to give a predominantly slipped arrangement. The degree of molecular slipping depends on the rigidity and the length of the connecting groups and on the substituents on the π-conjugated molecules. Face-to-face porphyrin dimers connected by two alkyl chains[13] and one rigid pillar, such as biphenylene, anthracene, dibenzothiophene, and dibenzofuran are discussed later on. 1,2-Phenylene-linked bisporphyrins give an open-mouth cofacial orientation.[15] The efficient synthesis of a series of 4,5-indenylene-linked porphyrin dimers by cobalt-mediated [2 + 2 + 2] cycloaddition of ethynylene-linked bisporphyrins and 1,6-heptadiyne has been reported recently.[16] The μ-oxodimer and double-decker porphyrins and phthalocyanines have a face-to-face orientation.[17]

Many head-to-tail dimers that have a strong electronic coupling have been constructed by direct linkages and connections through conjugate bridges. Porphyrin dimers linked directly at the *meso*–*meso* positions[18] are described later on. Other porphyrins linked directly at the *meso*–β[19] and β–β[20] positions have also been reported. These directly linked porphyrins can be transformed to form more conjugated, condensed aromatic systems by further oxidation.[21] Bisporphyrins linked through ethynylene,[22] ethenylene,[23] and 1,3-butadiynylene groups,[24] or others,[25] and bisphthalocyanines linked through ethynylene,[26] ethenylene,[27] or 1,3-butadiynylene[26] show significantly red-shifted absorption bands due to the effect of conjugation. The degree of electronic interaction depends on the torsional angle of the two π-conjugated molecules, and methods have been reported that can be used to control the torsional angle.[28]

The covalent approaches discussed above can be extended to prepare larger oligomers. A porphyrin trimer linked through 4,5-indenylene groups was synthesized by a cobalt-mediated double cyclization.[16a] Directly linked,[29] and ethynylene-[30] and 1,3-butadiynylene-linked[10,31] porphyrin oligomers have been constructed as products of a monodispersed distribution of molecular weights. Their structure–function relationship is useful for evaluating the coherence length of the singlet excited state and the charge delocalization length in the oligomers.

The dendritic approach is another method that has been used to construct multi-chromophoric architectures.[32] The characteristic functions of dendrons have been reported for many examples,[33] and although the exact control of the molecular orientation is difficult in these dendritic systems, the hierarchical shell structure is unique.

A non-covalent strategy allows for the formation of various types of assemblies. Although non-covalent bonds are considerably weaker than covalent bonds,[34] multiple or complementary interactions of non-covalent bonds can be used to stabilize a structure.[35] Coordination bonds are particularly strong amongst non-covalent bonds, and their interaction is generally directional. Complementary coordination of ligand-substituted zinc porphyrins gives structurally defined coordination dimers. Pyridyl-,[36] imidazolyl-,[35,37] pyrazolyl-,[38] and amino-substituted zinc porphyrins[39] give dimer, trimer, tetramer, and further assemblies, respectively. Some of these compounds are stable in concentrations below the micromolar level, and so can be treated as single molecules. The combination of coordination bonds and covalent bonds sometimes leads to giant supramolecular architectures, and examples of these will be discussed in a later section.

3. Molecular orientation of dimer motifs

How can we distinguish between H-aggregates and J-aggregates? (Fig. 2) First, we need to consider the orientation factor (κ) of the

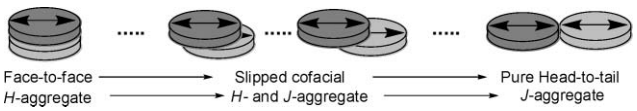

Fig. 2 Face-to-face and head-to-tail dimers and their intermediates.

dimers. The orientation factor between any two transition dipoles in a non-parallel orientation (Fig. 3) is defined by eqn (1)

$$\kappa^2 = (\cos\theta_T - 3\cos\theta_i\cos\theta_j)^2 \quad (1)$$

where θ_i and θ_j are the angles between the line connecting the centre of the two transition dipoles and each transition dipole moment, r is the centre-to-centre distance of the dipoles, and θ_T is the angle between the two transition dipole moments. The value of κ is always in the range 0–2.

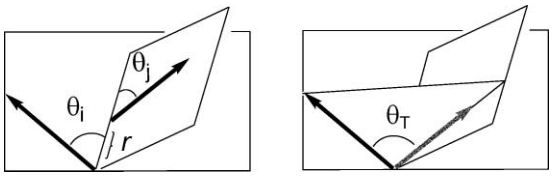

Fig. 3 Two transition dipoles in a non-parallel orientation.

When two transition dipoles exist in the same plane (an oblique conformation, see Fig. 4), the value of κ is given by eqn (2).

$$\kappa^2 = (\cos\theta_T - 3\cos^2\theta_i)^2 \quad (2)$$

In the case of a "slipped cofacial" system (Fig. 5), the value of κ is expressed by eqn (3). Two special cases are depicted as the "face-to-face" and "head-to-tail" cases for $\theta = 90°$ and 0°, respectively.

$$\kappa^2 = (1–3\cos^2\theta)^2 \quad (3)$$

The interaction of two transition dipoles causes a splitting of the absorption band, a so-called "excitonic coupling". The splitting energy, ΔE, is expressed by eqn (4)

$$\Delta E = \frac{2|M_1 M_2|\kappa}{r^3} \quad (4)$$

where M_1 and M_2 are the transition dipole moments for the transition in molecules 1 and 2, respectively, and r is the centre-to-centre distance between the two molecules. In the case of a homodimer, M_1 and M_2 are identical. Schematic images of the splitting energies in the face-to-face, head-to-tail, and oblique cases are shown in Fig. 6. Excitations to the lower energy state in the face-to-face orientation and to the higher energy state in the head-to-tail orientation are not observed as these are forbidden transitions. Split bands are observed in the oblique case.

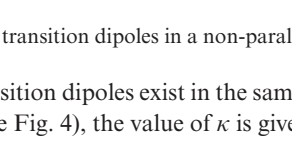

Fig. 4 Two transition dipoles in an oblique orientation.

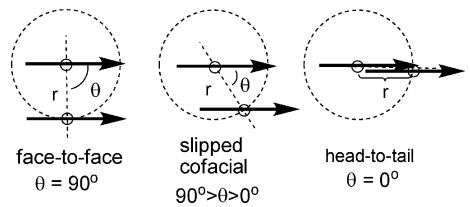

Fig. 5 Two transition dipoles in the "face-to-face" ($\theta = 90°$), "slipped cofacial" ($90 > \theta/° > 0$), and "head-to-tail" ($\theta = 0°$) orientations.

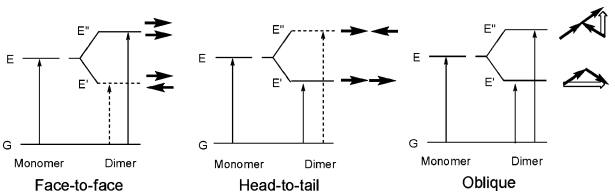

Fig. 6 Band splittings of face-to-face, head-to-tail, and oblique dimers.

When the angle θ is changed from 90° to 0° in a "slipped cofacial" system, the orientation factor varies as shown in Fig. 7. The data in Fig. 7 indicate that the orientation factor becomes zero at $\theta = 54.7°$, the so-called "magic angle". In the larger angle region ($90 > \theta/° > 54.7$), a blue-shifted band is observed, whereas a red-shifted band is observed in the smaller angle region ($54.7 > \theta/° > 0$). If the two molecules can rotate independently, then the average orientation factor of $\kappa^2 = 2/3$ ($\kappa = 0.8165$) is often used. Such a case is where two molecules are connected by a flexible alkyl chain. However, assembly systems tightly fixed by rigid connector(s) must consider the orientation factor. The UV–vis absorption band is sensitive to the orientation factor of closely connected molecular assemblies.

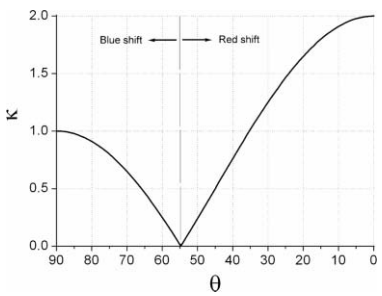

Fig. 7 The orientation factor, κ, in a "slipped cofacial" system as a function of angle, θ.

We will now consider porphyrin dimers. Porphyrins have a large Soret band (or B-band) occurring around 420 nm ($\varepsilon = 5.4 \times 10^5$ M^{-1} cm^{-1} ($\lambda_{max} = 424$ nm) for ZnTPP in toluene[40]). Due to the large transition dipole moment, changes in the Soret band spectra of porphyrin assemblies are frequently observed. D_4 symmetric metalloporphyrins have two orthogonal transition dipoles in the π-plane, and are degenerate in the monomeric state. In the case of *meso*-substituted porphyrins, the transition dipoles are set on the lines connecting the *trans meso–meso* positions, B_x and B_y, as shown in Fig. 8. D_4-symmetric metallophthalocyanines also have two degenerate transition dipole moments along the *trans* pyrrole–pyrrole directions.

When two porphyrins are placed in a space, then the first set of transition dipoles, B_x and B_y, interact with the second set of transition dipoles of the other porphyrin, $B_{x'}$ and $B_{y'}$. (Hereafter, the prime symbol denotes transition dipole moments belonging

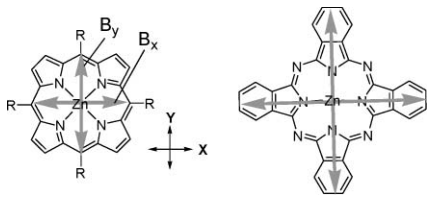

Fig. 8 Degenerate transition dipoles in D_4 zinc porphyrins and zinc phthalocyanines.

to the second molecule.) The observed absorption spectrum is the sum of the absorption bands resulting from the excitonic couplings. Therefore, if the orientation of the assembly is not fixed and has a distribution in space, then a broad Soret band is observed due to the presence of various types of interactions among B_x, B_y, B_x', and B_y'. However, in the case of a slipped cofacial porphyrin dimer, a relatively simple spectrum is observed, because of only two interactions occurring between B_x and B_x', and B_y and B_y'. Various covalently and non-covalently linked dimers are shown in Fig. 9, along with their corresponding monomers. These are classified into four types: (1) face-to-face (**1H$_2$-D** and **1Zn-D**),[41] (2) pure head-to-tail (**2**),[18b] (3) slipped cofacial (**4**,[42b,42d] **5**,[42] **6**,[43] **7**,[42] **8**,[43] **11D**,[36] **12D**,[37,44] **13D**[45]), and (4) non-parallel (**14**, **16**, **18**, and **20**[13a]). Based on experimental and molecular modelling data,[46] the orientation factor (κ), the interplanar distance ($b = r\sin\theta$), and the slip distance ($a = r\cos\theta$) of the dimers, except for the non-parallel case, can be estimated from the slip angle, θ, and the centre-to-centre distance, r (see Table 1). The definitions of r, θ, a, and b are shown in Fig. 10.

The crown ether-substituted phthalocyanine dimer **1-D** affords a face-to-face dimer. The angle, θ, is $\theta = 90°$, and the alignment

Table 1 Estimation of slip angles, centre-to-centre distances, π-electron overlapping, and orientation factors

	θ/deg	r/Å	a/Å	b/Å	κ	Ref.
1Cu$_2$-D	90[a]	4.1[b]	—	4.1	1	41
4H$_4$	81.7[c]	6.904[c]	0.997	6.832	0.94	42*b*
7H$_4$	63.8[c]	3.958[c]	1.747	3.551	0.42	42*b*
7Cu$_2$	65[c]	3.807[c]	1.632	3.500	0.46	42*a*
5Ni$_2$	58.3[c]	4.566[c]	2.399	3.885	0.17	42*a*
14Cu$_2$	—	6[b]	—	3.9[b]	—	13*a*
12D	33[a]	6.9[a]	5.79	3.23	1.11	35,47
11D	31[a]	6.73[a]	5.77	3.3	1.20	36
13D	25[a]	9.06[a]	8.21	3.83	1.46	45
2	0[a]	8.461[a]	—	—	2	18*b*

Estimated from[a] molecular modelling by Material Studio® (semi-empirical MO method, AM1), [b] ESR, and [c] single crystal analysis by X-ray.

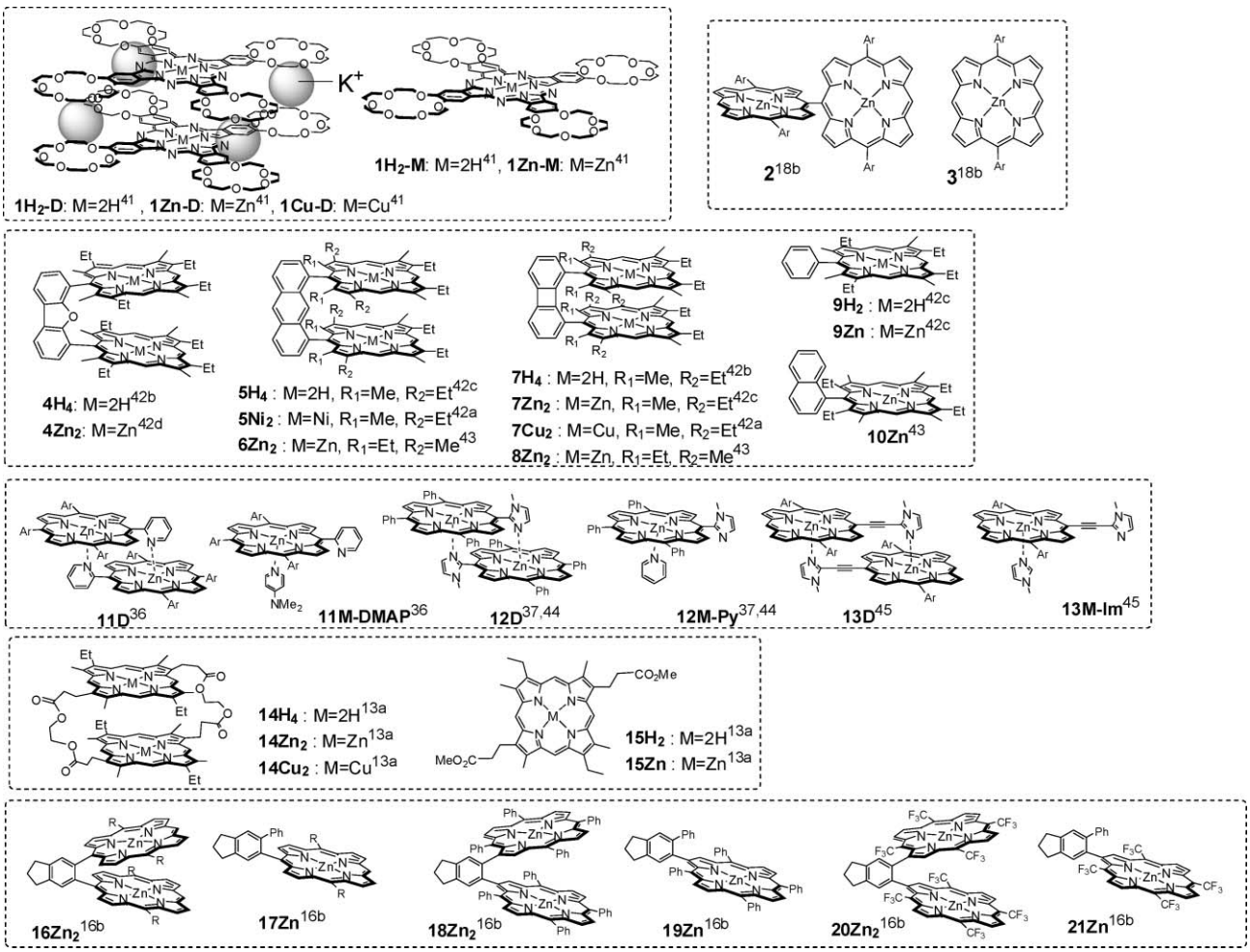

Fig. 9 Various dimer motifs of porphyrin–porphyrin and phthalocyanine–phthalocyanine homodimers.

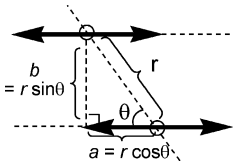

Fig. 10 Definitions of r, θ, a and b.

of the two transition dipole moments is perfect. The interphthalocyanine distance of **1Cu-D** was estimated to be 4.1 Å. The bisporphyrin linked directly at the *meso–meso* position, **2**, has a pure head-to-tail transition dipole, B_x–B_x' aligned along the bond line. Since the two porphyrin planes cannot be coplanar in this motif, the excitonic coupling between B_y and B_y' is small. In cofacial bis-β-substituted-porphyrins pillared by dibenzofuranylene (**4**), anthracenylene (**5** and **6**), and biphenylene (**7** and **8**), rotation along the connection bond is suppressed, keeping the two porphyrins coplanar. Even so, the two porphyrins can be slipped, and the angle depends on the structure of the pillars and the central metal ion. Compound **4H$_4$** has an open-mouth structure and a centre-to-centre distance of 6.9 Å,[42b] indicating that no π-electron overlap occurs. In the case of **7H$_4$**,[42b] **7Cu$_2$**[42a] and **5Ni$_2$**,[42a] the two porphyrin planes are slipped, and their interplanar distances are 3.55, 3.50, and 3.88 Å, respectively. The slip angles of compounds **4–8** are greater than 54.7°, and a blue shift of the Soret band is expected. In compounds **11D** and **12D**, the slip angles were estimated from molecular modelling to be 31° and 33°, respectively. The interplanar distances of **11D** and **12D** were determined to be 3.3 and 3.23 Å, respectively, from X-ray crystallography data.[35,34] Two pyrroles of one porphyrin overlap with the other two pyrroles in the other porphyrin molecule in both compound **11D** and compound **12D**. The slip angle is decreased to 25° when an ethynyl moiety is inserted, as in **13D**. In this case, the edge of the pyrrole molecules' π-electrons can still overlap. Structural analysis of **14** was carried out using NMR and ESR spectroscopy. The metal–metal and interplanar bond distances were estimated to be 6 and 3.9 Å, respectively. A series of bisporphyrins linked by a 4,5-indenylene moiety in **16Zn$_2$**, **18Zn$_2$**, and **20Zn$_2$** were classified as having a non-parallel orientation. The two porphyrins are located outside the indene moiety, and they can rotate along the connection bond. Their close positions can induce excitonic coupling and π-electron overlapping.

4. UV–vis absorption and fluorescence spectra of dimers

In this section, we discuss the UV–vis absorption and fluorescence properties of the dimers shown in Fig. 9. Table 2 lists the characteristic absorption bands, calculated excitonic coupling energy, and relative fluorescence intensity of dimers with respect to their corresponding monomers. In slipped cofacial systems, the observed absorption spectrum of the dimers is the sum of two interactions, B_x–B_x' and B_y–B_y'. As expected from the slip angles shown in Table 1, **4H$_4$**, **5H$_4$**, **7H$_4$**, **6Zn$_2$**, and **8Zn$_2$** show blue-shifted Soret bands as a result of two face-to-face interactions, B_x–B_x' and B_y–B_y'.

The splitting energies depend strongly on the interplanar distance of the two porphyrins. Thus, they increase in the order: **4H$_4$** < **5H$_4$** < **7H$_4$** and **6Zn$_2$** < **8Zn$_2$**. The relative fluorescence intensity decreases in the same order, *i.e.*, the larger splitting energy systems showing the smallest fluorescence intensities. In particular,

Table 2 UV–vis absorption and fluorescence data

	Solvent	λ_{max}nm	cm^{-1}	ΔE/cm^{-1}[a]	Fluorescence[a]	Ref.
1Zn-M	$CHCl_3$	677	14 771	—	—	41
1Zn-D	$CHCl_3$[b]	635	15 748	−977	—	
1H$_2$-M	$CHCl_3$	662	15 105	—	1	41
		700	14 285	—		
1H$_2$-D	$CHCl_3$[b]	639	15 649	—	~0	
9H$_2$	MTHF[c]	402	24 875	—	1	42*c*
4H$_4$	MTHF	396	25 252	−377	1.05	
5H$_4$	MTHF	395	25 316	−441	0.22	
7H$_4$	MTHF	379	26 385	−1510	0.04	
10Zn	CH_2Cl_2	405.5	24 660	—	1	43
6Zn$_2$	CH_2Cl_2	392	25 510	−849	0.33	
8Zn$_2$	CH_2Cl_2	388	25 773	−1112	~0	
15H$_2$	CH_2Cl_2	397	25 188	—	1	13*a*
14H$_4$	CH_2Cl_2	387	25 839	−651	0.47	
15Zn	CH_2Cl_2	402	24 875	—	1	
14Zn$_2$	CH_2Cl_2	388	25 773	−898	0.15	
12M-Py	$CHCl_3$	427.9	23 370	—	1	47
12D	$CHCl_3$	415.3	24 079	−709	~1	
		434.2	23 031	339		
11M-DMAP	CH_2Cl_2	428.4	23 340	—	—	36
11D	CH_2Cl_2	413.2	24 200	−860	—	
13M-Im	$CHCl_3$	431.0	23 200	140	—	
		443.5	22 548	—	—	45
13D	$CHCl_3$	434	23 041	−494	—	
3	THF	413	24 213	175	1	18*b*,29
2	THF	416	24 038		1.3	
		451	22 173	2040		

[a] Relative to monomer. [b] CH_3CO_2K in $CHCl_3$ containing 0.1 v/v% of MeOH. [c] 2-MeTHF.

none or only a faint fluorescence is observed in **$1H_2$-D** and **$8Zn_2$**. Exceptionally, the fluorescence intensity of **$4H_4$** was almost same as that of the corresponding monomer, even though the absorption band was blue-shifted. The tetraesters **$14H_4$** and **$14Zn_2$** show blue-shifted Soret bands, and both fluorescences are significantly quenched. These results indicate that strong π-electron overlap in face-to-face dimers produces non-fluorescence decay processes. In the case of the slipped cofacial dimers **11D** and **12D**, both blue-shifted and red-shifted Soret bands are observed from face-to-face B_y–B_y' and slipped cofacial B_x–B_x' interactions, respectively (see Fig. 11). The red-shifted peak is consistent with the slip angle (<54.7°). In the case of **12D** and other imidazolyl-zinc-porphyrin dimers, no fluorescence quenching was observed with respect to the corresponding monomers. This remarkable feature is associated with this motif, even though a significant π-electron overlap exists. No fluorescence spectrum has been reported for other complementary coordination dimers, probably because the dimer structure cannot be maintained under micromolar concentrations to measure the steady state fluorescence spectra. Because the imidazolyl-zinc-porphyrin dimer has a very large self-association constant ($K > 10^{11}$ M^{-1} in $CHCl_3$),[47] it can be treated safely under micromolar concentrations. This is another unique property of this series of complementary coordination dimers. The UV–vis absorption spectrum of the *meso–meso*-linked porphyrin **2** also shows a split Soret band as a red-shifted and a non-interactive peak. The relative fluorescence of **2** is stronger than that of the monoporphyrin **3**.[29] Direct connection at the *meso–meso* position is useful for expansion of the absorption range without any associated fluorescence quenching.

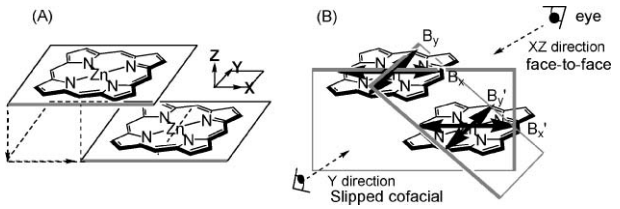

Fig. 11 A slipped cofacial porphyrin dimer model (A) and its transition dipole moment (B).

In face-to-face dimers (*i.e.*, H-aggregates), fluorescence quenching is generally observed using various dyes. The mechanism can be explained as follows. As shown in Fig. 6 for the face-to-face case, the forbidden state of transition vectors orientated in opposite directions lies below the allowed state of transition vectors orientated in the same direction. The higher excited state is rapidly converted to the lower excited state. Due to the forbidden nature of the radiative decay from the lower excited state to the ground state, intersystem crossing or other non-radiative decay processes dominate, resulting in little or faint fluorescence emissions. In some cases, fluorescence from the forbidden low excited state is observed.[48] Würthner recently reported on a fluorescent H-aggregate of a merocyanine dye, in which the fluorescence from the forbidden excited state was clearly observed at wavelengths different from the fluorescence from the residual monomer.[49] In this case, the fluorescence from the monomer was very weak, which is probably due to bond-twisting.

The formation of a rigid H-aggregate suppresses the non-radiative decay process caused by bond-twisting. In the case of the face-to-face porphyrin dimers **4–8**, a blue-shifted absorption band is observed only for the Soret band (*i.e.*, the S2 level). In the S1 area, significant fluorescence quenching occurs for face-to-face dimers due to the same mechanism as above, although the forbidden nature of the S1 transition obscures the blue- and red-shifts. In the complementary coordination dimer **12D**, the lower excited state produced by the transition dipole interaction of B_y–B_y' is forbidden, whereas that of B_x–B_x' is allowed. The former forbidden state is rapidly converted to the latter allowed state by an intrachromophoric dipole equilibrium,[50] which results in an intrinsic fluorescence emission. This allows the use of both blue- and red-shifted absorption bands for light harvesting.

An increase in chromophore size tends to induce random aggregation, which generally produces energy sinks that quench the fluorescence. Molecular wrapping of single rod-like chromophores by dendritic substituents has been proposed as an effective method to prevent random aggregation.[51] In supramolecular assemblies, the continuous growth of the structure avoids the formation of any energetic heterogeneity, and ensures light-harvesting antenna functionality.

5. Effect of substitution on the splitting of the Soret band

As described in the previous section, imidazolyl-zinc-porphyrins are good motifs showing split Soret bands and strong electronic coupling without any fluorescence quenching. The shape of the Soret band changes significantly, depending on the substituent group on the porphyrin. In this section, the relationship between the structure and the width of the Soret band splitting and the shape of the Soret band is discussed.

The structure of several imidazolyl-zinc-porphyrin dimers and their UV–vis absorption spectra are shown in Fig. 12 and 13, respectively. The triphenyl-substituted porphyrin **12D** shows a split Soret band at 415.3 and 434.2 nm. These are blue- and red-shifted from the Soret band of **12M-Py** (427.9 nm). The splitting energies of **12D** with respect to the monomer **12M** were calculated to be -709 cm^{-1} for the B_y–B_y' interaction ($\kappa = 1$) and 339 cm^{-1} for the B_x–B_x' interaction ($\kappa = 1.1$), respectively. Compound **12D** is considered to be a standard dimer in a series of imidazolyl-zinc-porphyrin dimers, because the magnitudes of the two transition dipoles, B_x and B_y, is considered to be similar and nearly degenerate. The half-bandwidth of the Soret bands of **12M-Py** and pyridine-coordinated zinc tetraphenylporphyrin (**ZnTPP-Py**) is almost the same, indicating that **12M-Py** has a pseudo C_4 symmetry for the π-electronic system of the porphyrin.

When the *meso*-phenyl substituents along the B_y direction are replaced by aliphatic substituents (**22D**),[52] then the coupling energies of both the B_y–B_y' and B_x–B_x' interactions increase to -879 and 349 cm^{-1}, respectively. The intensity of the Soret band at longer wavelengths increases relative to the intensity of the short wavelength Soret band. When the last phenyl group in **22D** is further replaced by a ferrocenyl group, then the split Soret bands become more unsymmetrical (**23D**).[52] The intensity of the longer wavelength band increases significantly. The coupling energy of the B_x–B_x' interaction increases slightly to 524 cm^{-1}, whereas the coupling energy of the B_y–B_y' interaction decreases significantly to -549 cm^{-1}. The ferrocenyl group is an electron-donating

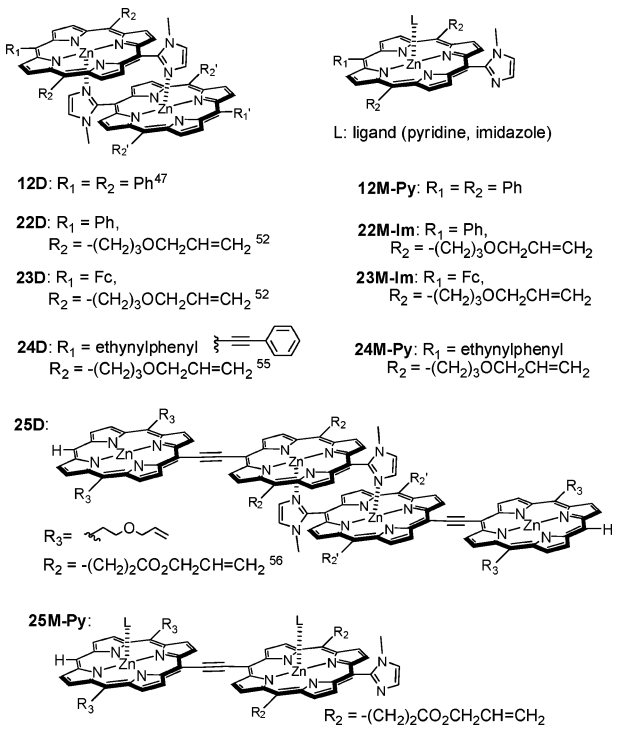

Fig. 12 Various imidazolyl-zinc-porphyrin dimers and the corresponding monomers.

substituent and the steric requirement for the coplanar orientation is small compared with six-membered aromatic substituents. The coplanarity and the electronic coupling interactions between the ferrocenyl and the porphyrin moieties can increase. Such an asymmetric substitution generally disrupts the degeneracy of the two transition dipoles. In fact, the Soret band of the corresponding monomer **23M-Im** is broader than the Soret bands of **12M-Py** and **22M-Im**. Such a disruption of the degeneracy becomes more obvious in the monomeric phenylethynyl-substituted porphyrin, **24M-Py**.[53] Thus, two Soret bands corresponding to B_y and B_x are observed at 433.6 and 445.8 nm as low- and high-intensity peaks, respectively. The Soret and Q(0,0) bands are significantly red-shifted due to the increase in π-electron conjugation. When the dimer forms, almost no shift is observed for the B_y–B_y' interaction, and a relatively small red shift (386 cm^{-1}) is observed for the B_x–B_x' interaction. The reason for the small coupling energy is unclear. A possible explanation is that the distance between the two dipole moments is further increased by an expansion of the conjugated π-electron system, even though the centre-to-centre distance between the two porphyrins remains the same. When another zinc porphyrin is connected through an ethynylene unit, then Soret bands at longer wavelengths appear at 485 and 493 nm for monomer **25M-Py** and dimer **25D**, respectively.[54] The coupling energy (335 cm^{-1}) is relatively small compared to cases for other dimers. Here again, the expansion of the π-electron system along the B_x direction decreases the coupling energy of the complementary coordination dimer, although the magnitude of the transition dipole moment, B_x, must be increased. In the imidazolylethynyl-zinc-porphyrin dimer, **13D**, the centre-to-centre distance becomes longer than that of the imidazolyl-zinc-porphyrin dimers. The UV–vis absorption spectrum of **13D** shows a broad Soret band instead of split peaks. In contrast to other imidazolyl-zinc-porphyrin systems, the Soret band is red-shifted for the dissociated monomer **13M-Py** rather than the dimer **13D**. This shift results from a conformational change of the imidazolyl group, which is oriented perpendicular to the attached porphyrin in the coordination dimer, and becomes coplanar in the dissociated monomer.

6. Polymeric and macrocyclic systems using complementary coordination

The combined use of covalently and non-covalently linked dimer motifs provides for well-oriented oligomeric and polymeric systems. The resulting absorption spectra are expanded to capture a wide wavelength range of visible light, and the excitation energy can be transferred over a long distance through the chain. The application of complementary coordination motifs **12D** and **13D** to the *meso–meso* linked dimer **2** gives **26P**[47,55] and **27P**[45] (see Fig. 14). These are dissociated into monomeric species **26M-Py** and **27M-Py** in the presence of excess pyridine. In non-coordinating solvents, such as $CHCl_3$, CH_2Cl_2, and toluene, polymeric **26P** and **27P** are produced spontaneously. The number of assembly units is

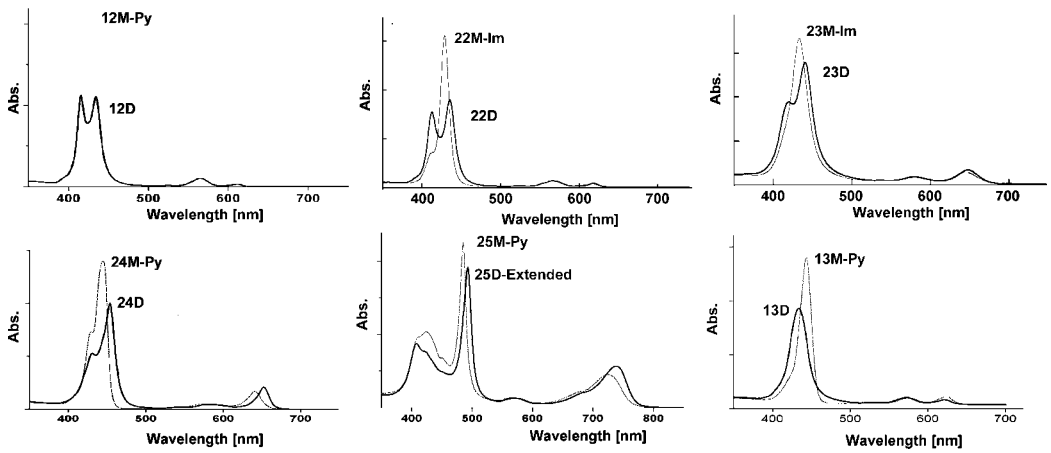

Fig. 13 UV–vis absorption spectra of **12M-Py**, **12D**, **22M-Im**, **22D**, **23M-Im**, **23D**, **24M-Py**, **24D**, **25M-Py**, **25D-Extended**, **13M-Py**, and **13D**. (Key: dimer = black, monomer = grey.)

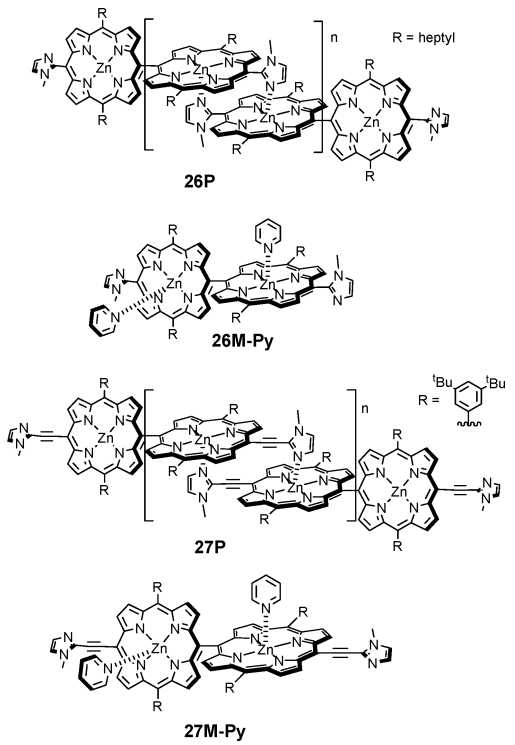

Fig. 14 Complementary coordination polymers **26P** and **27P**, and the unit molecules.

dependent on the concentration. The average number has been estimated to produce more than a 700-mer for **26P** in $CHCl_3$ from gel permeation chromatography (GPC) data, and a 45-mer for **27P** in 5.8×10^{-5} M $CHCl_3$ from the self-association constant.

The absorption spectrum of polymer **26P** shows split Soret bands at 408.5 and 489.5 nm, which are blue- and red-shifted by −528 and 1357 cm^{-1}, respectively, compared to the Soret band of the corresponding monomer **26M-Py** (Fig. 15). Polymeric **27P** also shows split Soret bands at 432 and 490.5 nm, whereas the dissociated monomer **27M-Py** shows split Soret bands at 437 and 473.5 nm. The absorption spectrum of both polymers covers a wide wavelength range of visible light. The fluorescence spectrum of polymeric **26P** does not show any obvious quenching,[55] indicating a potential use in light-harvesting antennae. The fluorescence was quenched efficiently when an acceptor molecule was introduced at the terminal position.[47] This means that excitation takes place at any location in the assembly, and that the energy is transferred to the terminal acceptor.

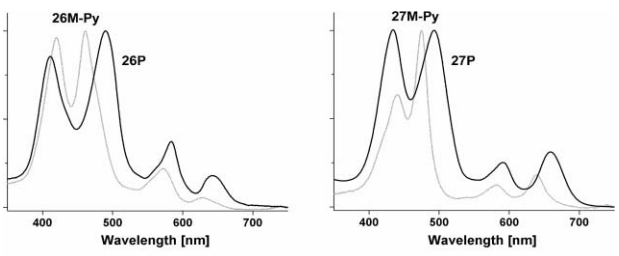

Fig. 15 UV–vis absorption spectra of **26M-Py**, **26P**, **27M-Py**, and **27P**. (Key: polymer and dimer = black, monomer = grey.)

When complementary dimer motifs are connected by non-linear spacers, macrocyclic oligomers are produced spontaneously under diluted conditions without the formation of polymeric side products. The size of the macroring is easily controlled by the angle between the two connecting bonds. In the case of *m*-phenylene-linked bis(imidazolyl-zinc-porphyrins), pentameric and hexameric supramolecular macrorings, **C-P5** and **C-P6**, are formed[56] (Fig. 16). To determine the exact assembly number using mass spectrometry, the macrorings were covalently linked using a ring-closing metathesis reaction.[56b,57] The covalently linked macrorings did not dissociate under the conditions used in the mass spectrometer, not even when using coordinating solvents, such as pyridine. Two different sized macrorings were separated using GPC.

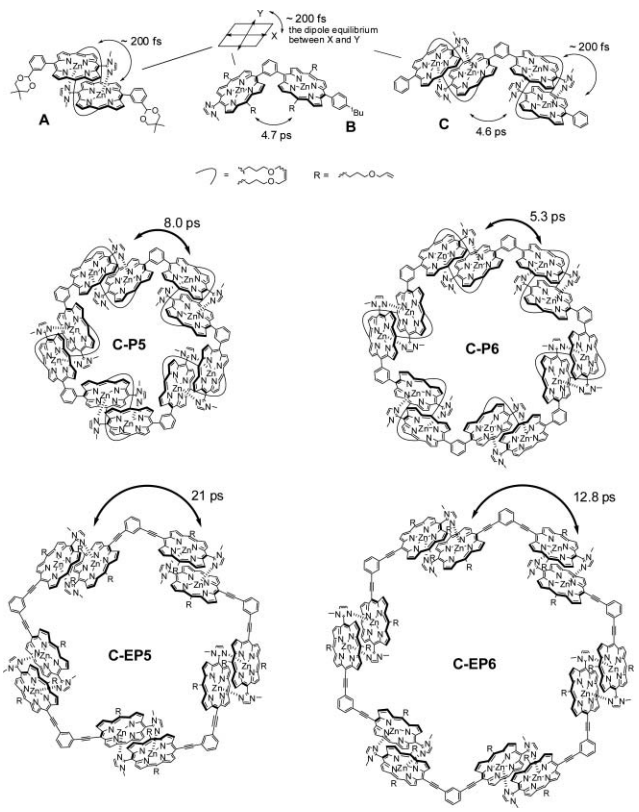

Fig. 16 Supramolecular porphyrin macrorings **C-P5**, **C-P6**, **C-EP5**, and **C-EP6** with reference porphyrins **A**, **B**, and **C**.

The photophysical dynamics of **C-P5** and **C-P6** were determined using reference porphyrins **A**, **B**, and **C** through nanosecond time-resolved fluorescence and fluorescence decay anisotropy, and femtosecond transient absorption (TA) and transient absorption anisotropy (TAA).[58] The fast excitation-energy hopping (EEH) rates in the rings were also determined using the latter two methods. The TAA decay reflects the depolarization of the exciton that is initially localized in weakly coupled multi-chromophores. The EEH parameters between the two zinc porphyrin monomers in the cofacial dimer and the cofacial porphyrin dimers in the macrorings were obtained from the data. Exciton–exciton annihilation processes occur in light-harvesting antenna systems under multi-photon absorption conditions. These processes are also associated with the EEH value.[59] Pump power-dependent

transient absorption experiments give related parameters used to calculate the value of the EEH.

The TAA decay of **A** shows only a single component with a time constant of ~200 fs. The fast component originates at the dipole equilibrium of the zinc porphyrin monomer, and the EEH originates between the zinc porphyrin monomers in the cofacial dimer. The TAA decay of **B** and **C** was fitted using two components with time constants of *ca.* 200 fs and 4.6 ps, respectively. The faster component was assigned the same value as that of **A**, and the slower component was assigned the same value as EEH between the two zinc porphyrin monomers of **B**, and the two cofacial zinc porphyrin dimers of **C**. In the case of **C-P5** and **C-P6**, the two decay components were obtained in a similar manner. The slower time constants of 2.11 ps for **C-P5** and 1.62 ps for **C-P6** are similar to those obtained for **C**. These values were used to calculate the EEH values of the macrorings. At the same time, the pump power-dependent TA was measured for **C-P5** and **C-P6**, along with references **A** and **B**. The TA decay of **C-P5** and **C-P6** was very sensitive to the pump power, whereas no pump power dependence was observed for references **A** and **B**. This indicates that the exciton–exciton annihilation between the cofacial dimer units occurred only in ring structures of **C-P5** and **C-P6**. The EEH processes were analysed based on a Förster-type energy-transfer model, assuming a migration-limited character of the exciton–exciton annihilation and a random-walk formalism for the anisotropy decay. The EEH time was obtained using eqn (5) and (6), in which N was the number of EEH sites, a was the angle between the neighbouring transition dipoles, $\tau_{\text{annihilation}}$ was the slowest exciton–exciton annihilation time, and τ_{hopping} was the inverse of the nearest neighbour energy-hopping rate.[60]

$$\tau_{\text{depolarization}} = \frac{\tau_{\text{hopping}}}{4(1-\cos^2(2\pi/N))} = \frac{\tau_{\text{hopping}}}{4(1-\cos^{2a})} \quad (5)$$

$$\tau_{\text{annihilation}} = \frac{N^2-1}{24}\tau_{\text{hopping}} \quad (6)$$

For values of $N = 5$ and $a = 72°$ for **C-P5**, and $N = 6$ and $a = 60°$ for **C-P6** in eqn (5) and (6), the values of $\tau_{\text{depolarization}} = 7.6$ ps for **C-P5** and $\tau_{\text{depolarization}} = 4.9$ ps for **C-P6**, and $\tau_{\text{annihilation}} = 8.3$ ps for **C-P5** and $\tau_{\text{annihilation}} = 5.7$ ps for **C-P6**, respectively, were obtained. It should be noted that both of the time constants obtained from the two different experiments were the same within a small error range (*i.e.*, for the EEH times, this was 8.0 ± 0.5 ps for **C-P5** and 5.3 ± 0.6 ps for **C-P6**), which validates the treatment.

Two larger macrocycles **C-EP5** and **C-EP6** were synthesized to examine further the relationship between the macroring structure and the EEH times.[53] In these motifs, the cofacial dimer units are connected through a 1,3-bisethynylenephenylene moiety. Their structural analysis was carried out using ^{1}H NMR spectroscopy, mass spectrometry, and high-resolution scanning tunnelling microscopy (HRSTM).[61] The simple NMR spectra of non-metathesized **EP-5** and **EP-6** indicate that the rotation of the dimer units along the ethynylene bonds is fast, occurring within the NMR timescale. This may contribute to a strong electronic coupling between two cofacial dimer units.

The photophysical dynamics of **C-EP5** and **C-EP6** were examined using the same methods as used for **C-P5** and **C-P6**. The EEH times within the macrorings of **C-EP5** and **C-EP6** were determined to be 21 ps for **C-EP5** and 12.8 ps for **C-EP6**. A comparison of these data with those from the *m*-phenylene-linked macrocycles, **C-P5** (8.0 ps) and **C-P6** (5.3 ps), suggests that the EEH time depends on the distance of the hopping sites. Although in **C-EP5** and **C-EP6**, both coplanarity and electronic communication through the ethyne bond were introduced, the apparent EEH times were increased. The ethyne moiety between the porphyrin and phenylene brings about a red-shift of the absorption spectra of **C-EP5** and **C-EP6** compared to **C-P5** and **C-P6**. In addition, the Q(0,0) band intensity of **C-EP5** and **C-EP6** are significantly higher. These features may play an important role as a second antenna into which excitation energy can be funnelled from surrounding higher energy antenna. Since the emission spectra of **C-P5** and **C-P6** overlap with the absorption spectra of **C-EP5** and **C-EP6**, their composite systems may provide an energy cascade system, such as LH2 and LH1.

Interestingly, the EEH times of the hexameric macrorings of **C-P6** and **C-EP6** are faster than those of the corresponding pentameric macrorings of **C-P5** and **C-EP5**. In Förster-type energy transfer, the rate constant is expressed by eqn (7), in which n is the refractive index of the solvent, R is the centre-to-centre distance between the donor and the acceptor, τ is the fluorescence lifetime of the energy donor, κ is the orientation factor, Φ is the fluorescence quantum yield, and J is the spectral overlap integral.

$$k_{\text{TS}} = \frac{8.8 \times 10^{-25}\kappa^2\Phi}{n^4R^6\tau}J \quad (7)$$

If we assume perfectly planar structures for the pentagons and hexagons, then the orientation factor, κ, is calculated to be $\kappa = 1.65$ for **C-P5** and **C-EP5** and $\kappa = 1.75$ for **C-P6** and **C-EP6**. The centre-to-centre distances between the two cofacial dimer units were estimated from molecular modelling to be 15.5, 16.1, 19.9, and 20.7 Å for **C-P5**, **C-P6**, **C-EP5**, and **C-EP6**, respectively. With respect to the distances between the energy-hopping sites, the hexamers **C-P6** and **C-EP6** are less favourable than the pentamers **C-P5** and **C-EP5** by a factor of 1.04, whereas they are more favourable by a factor of 1.06 with respect to the orientation factor. Since the energy transfer rate is affected by the inverse of the sixth power of the separation distance and is proportional to the square of the orientation factor, then the decrease in the rate constant of the hexamers due to the longer distance ($1/(1.04)^6 = 0.79$) seems to dominate over the increase due to the orientation factor ($(1.06)^2 = 1.12$). However, both EEH rates of the hexamers **C-P6** and **C-EP6** are faster than those of the corresponding pentamers, **C-P5** and **C-EP5**. This suggests that hexameric structures have a better orientation, which is probably due to the strong electronic coupling or accumulated hopping.

Other supramolecular porphyrin macrorings can be obtained by changing the spacer structures.[62] When a ferrocenyl group was used as a spacer, a series of giant macrorings were obtained.[63] The ring sizes were estimated using well-resolved GPC peaks and the result was finally confirmed by HRSTM.[64]

Covalently linked **C12ZA**[65] and **C24ZB**[66] have been synthesized recently, and their photodynamic properties have been examined using the same methods as applied to the above macrorings (Fig. 17). In these motifs, the EEH times among the *meso–meso*-linked dimer or tetramer units in **C12ZA** and **C24ZB** are very fast (*ca.* 240 fs), suggesting that coherent units exist. The EEH times

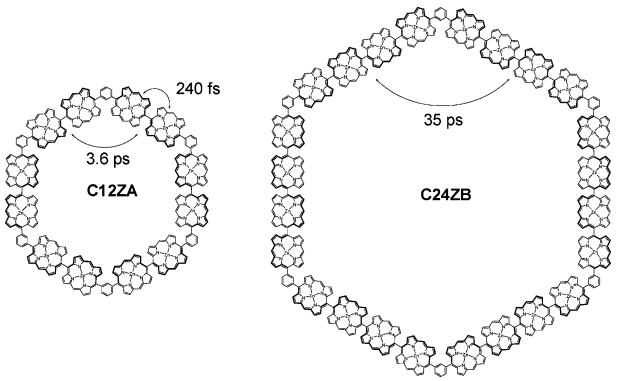

Fig. 17 Porphyrin macrorings of **C12ZA**[65] and **C24ZB**.[66]

between the dimer and the tetramer units were estimated to be 3.6 and 35 ps for **C12ZA** and **C24ZB**, respectively. Since the centre-to-centre distance between the energy hopping sites of **C24ZB** is roughly 1.5 times longer than that of **C12ZA**, then the slower time constants observed in **C24ZB** are consistent with the above explanation ($1/(1.5)^6 = 0.09$). Similar to **B850**, the transition dipoles in the macrocyclic rings of **C-P5**, **C-P6**, **C-EP5**, **C-EP6**, **C12ZA**, and **C24ZB** are aligned along the ring axis. The well-ordered orientation must contribute to the efficient excitation energy transfer in the rings.

Since the zinc(II) ion is limited to five-coordination, the polymerization of the monoporphyrin unit cannot be achieved using a complementary coordination strategy. Replacement of the zinc(II) ion by metal ions permitting six-coordination must consider two factors: the large stability constant and the zero fluorescence quenching required to obtain stable assemblies for light-harvesting functions. The use of Co(III) porphyrin **29** (see Fig. 18) only satisfies the former condition, and giant J-type assemblies are obtained without any fluorescence emission.[67]

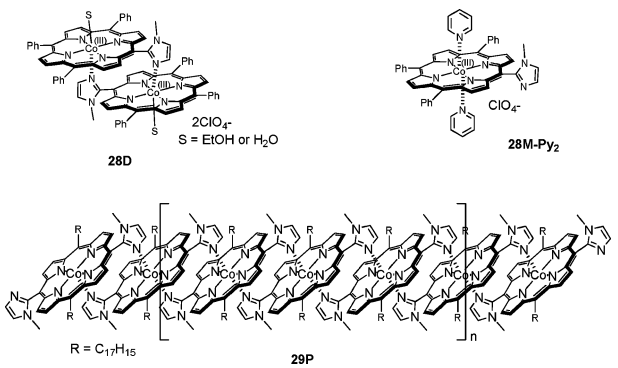

Fig. 18 Complementary coordination dimer **28D**, polymer **29P**, and the monomer **28M-Py$_2$**.

The absorption spectrum of the dimer **28D** (see Fig. 19) shows a broad Soret band with respect to that of the corresponding monomer, **28M-Py$_2$**. However, the splitting energy of the dimer **28D** is smaller than that of imidazolyl-zinc-porphyrin dimers **12D** and **22D**.[67b,68] When **29P** is formed, the Soret band appears with a large split width at 402 and 478 nm.† The difference in energy

† Polymerization of **29** usually accompanies a shorter oligomer, but the absorption spectrum of long polymer **29P** was obtained in the course of analytical gel permeation chromatography by photodiode array detector.

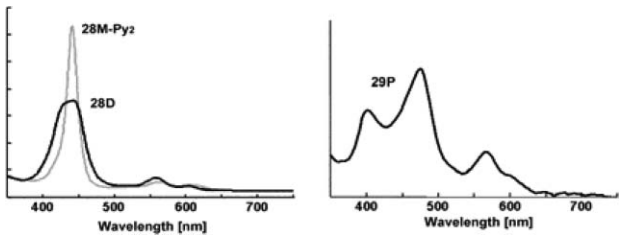

Fig. 19 UV–vis absorption spectra of **28M-Py$_2$**, **28D**, and **29P**. (Key: polymer and dimer = black, monomer = grey.)

of the Soret band from the monomer, **28M-Py$_2$**, is −2200 and 1755 cm^{-1}, indicating that both B_x–B_x' and B_y–B_y' interactions are accumulated in this system. Compound **29P** is a unique example of a coordination-organized large J-aggregate with a significant π-electron overlap, and so this compound may be used as a charge transporter.

7. 2-Pyridinyl-zinc-chlorin and imidazolyl-zinc-phthalocyanine dimers

In porphyrin assemblies, strong excitonic couplings are observed, mainly in the Soret band, whereas the coupling energy of the Q-band is generally small. This result comes from the smaller oscillator strength of Q-bands. In natural photosynthetic systems, partly hydrogenated porphyrins such as chlorin and bacteriochlorin are used in light-harvesting antenna systems.[69]

Due to the removal of the degeneracy of the two transition dipoles, the Q(0,0)-band becomes much more intense than that of porphyrin. However, the complementary coordination dimer of (2-pyridinyl)-zinc-chlorin, **30D**, exhibits only a small red-shift of the Q-band (70 cm^{-1})[70] (Fig. 20).

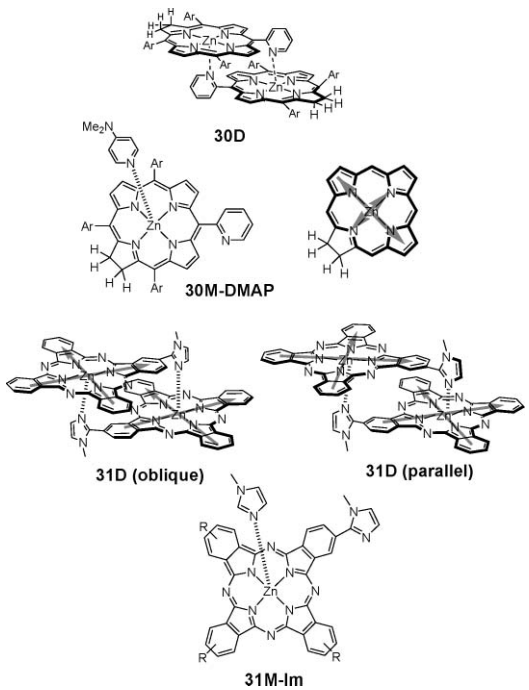

Fig. 20 (2-Pyridinyl) chlorin, **30**, and the imidazolyl-zinc-phthalocyanine dimer, **31**.

D_4-Metallophthalocyanine has two degenerate transition dipoles along the axis connecting the two *trans* benzopyrroles, but the intensity of the Q(0,0)-band is much larger than that of porphyrin. The molar extinction coefficient ($\varepsilon = 2 \times 10^5$ M^{-1} cm^{-1} (677 nm in toluene) for **Zn′BuPc**) is large enough to induce a significant excitonic coupling. We recently succeeded in synthesizing β-substituted imidazolyl-zinc-phthalocyanines **31**.[71] Similar to the imidazolyl-zinc-porphyrins, **31** affords the complementary coordination dimer **31D**. In this case, two structural isomers, oblique and parallel, were observed in the ^{1}H NMR spectra using a non-symmetrical disposition of the imidazolyl substituent. The absorption spectrum of the dimer mixture shows split Q-bands at 669.5 and 699 nm with respect to the absorption spectrum of the monomer (679 nm). The apparent splitting energies are −209 and 421 cm^{-1}, respectively. In contrast to the porphyrin dimer, the shift of the Soret band, occurring around 350 nm, is negligible. The fluorescence quantum yield of the dimer is almost the same as that of the monomer, indicating once again that complementary coordination does not quench the fluorescence.

Other phthalocyanine dimers with covalent and non-covalent linkages have been reviewed previously.[72] Covalently linked systems with direct[73] connections or through cyclophane-type,[74] shared phenylene,[75] and ethynylene groups[26] seem to be potential candidates for both light-harvesting and charge transport. A combination of covalent dimers with complementary coordination motifs may provide phthalocyanine polymers, as in the case of porphyrins.

8. Porphyrin–phthalocyanine heterodimers

Porphyrin–porphyrin and phthalocyanine–phthalocyanine homodimers have been discussed in the previous sections. Since the two molecules are identical in these cases, the excitonic interaction leads to a clear splitting of the Soret or Q-bands. Here, we will discuss cases involving a closing connection with a porphyrin and phthalocyanine link.[76] Large spectral changes are observed for various face-to-face porphyrin–phthalocyanine heterodimers constructed from electrostatic and hydrophobic π–π interactions in aqueous or very polar media.[77] The shape of the absorption spectra depends on the nature and the combination of the central metal ions of the porphyrin and the phthalocyanine. Recently, two head-to-tail porphyrin–phthalocyanine heterodimers, **32** and **33**, have been reported by our group[78] and Torres′ group[79] (see Fig. 21). A direct linkage at the *meso*- or β-positions of the porphyrin and the β-position of the phthalocyanine restricts free rotation along the connecting bond. In the UV–vis absorption spectra of these heterodimers, the Q(0,0) band of the phthalocyanine moiety is red-shifted and is broadened significantly when compared to the Q(0,0) band of monomeric phthalocyanine.

Both energy and electron transfer occur in porphyrin–phthalocyanine heterodimers. The direction of the energy transfer always occurs from the porphyrin to the phthalocyanine, but electron transfer occurs from either side, depending on the redox potential of the two moieties. Interestingly, although the energy gap of the charge separation is very small, the electron transfer occurs smoothly in polar media. We recently examined the photoinduced charge separation of the porphyrin–phthalocyanine heterodimer **32D** using ultra-fast transient absorption spectra.[80] In this case, electron transfer occurred from the excited zinc

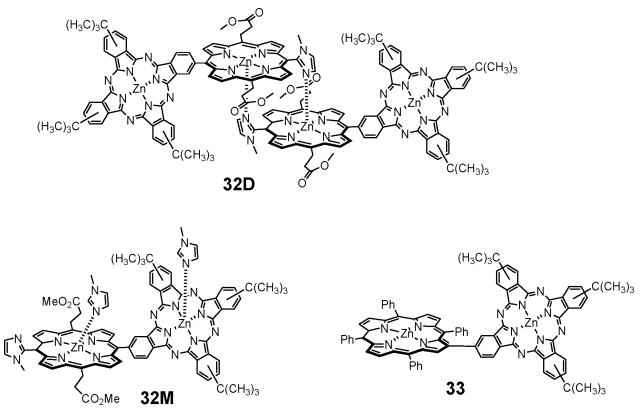

Fig. 21 Porphyrin–phthalocyanine heterodimers, **32** and **33**.

phthalocyanine to the zinc porphyrin. Even if the porphyrin part is excited selectively, this vectorial electron transfer occurs after a singlet energy transfer from the excited porphyrin moiety to the adjacent phthalocyanine part. Since the absorption bands of **32D** cover a wide range of the visible part of the spectrum, any visible light produces a charge separated state. It is noteworthy that the energy gap between the charge separated state (1.84 eV) and the excited phthalocyanine state (1.8 eV) is very small. This means that a high-energy hole–electron pair is efficiently generated in the charge separated state. A separation of this high-energy ion pair in the opposite direction produces both high-lying oxidants and reductants, as targets for artificial photosynthesis.

9. Outlook

In this article, we have focused on assemblies of porphyrins and phthalocyanines with strong electronic coupling in well-defined orientations. Complementary coordination motifs are satisfactory in every respect in terms of structural stability, orientation factor, π-electron overlap, and zero fluorescence quenching. The range of absorption wavelengths can be adjusted and expanded on by choosing unit molecules and polymeric extensions. In fact, the entire visible range of the spectrum can be covered by a combination of *meso–meso*-linked bisporphyrin polymers, **26P** and **27P**, and the phthalocyanine dimer **31D**. At the same time, the one-dimensional porphyrin polymer **26P** acts as a singlet energy transporter. Polymer **26P**, which is composed of charge resonance interacting pairs[81] and a *meso–meso*-linked porphyrin, leads to an efficient charge separation and charge transporter. A polymer combining these features may act as a charge transporter.[82] In the final sections, the porphyrin–phthalocyanine heterodimer **32D** was shown to provide a unique reaction centre, in which the excited singlet energy funnelled from both chromophores is converted to a high-energy electron–hole pair.

Biomimetic research has succeeded in constructing each functional unit, antenna, and reaction centre. The connectivity, as illustrated in Fig. 1, remains a challenging target. Here, the source and drain of the electron are separated from each other by only the membrane thickness. Therefore, successful achievement of a biological mimic of photosynthesis depends on a two-dimensional arrangement of each energy-producing unit. On the other hand, artificial energy-producing machines may combine the above

elements and achieve the following tasks successively: (1) light-harvesting over the entire range of visible light, (2) transport of excited energy to a reaction centre, (3) charge separation to produce a high-energy electron–hole pair, and (4) charge transport to opposite directions to supply the charges for external terminals. Since the two terminals are separated by long distances to prevent charge recombination, the object of future work is to overcome the problem of how to convey the excitation energy, electrons, and holes over extended electrode distances.

Acknowledgements

We greatly appreciate reviewers' helpful comments. This work was supported by Young Scientists (B) (AS) and Grants-in-Aid for Scientific Research (A) (YK) from the Japan Society for the Promotion of Science (JSPS).

References

1 (*a*) G. McDermott, S. M. Prince, A. A. Freer, A. M. Hawthornthwaite-Lawless, M. Z. Papiz, R. J. Cogdell and N. W. Isaacs, *Nature*, 1995, **374**, 517–521; (*b*) C. Jungas, J.-L. Rananck, J. L. Rigaud, P. Joliot and A. Vermeglio, *EMBO J.*, 1999, **18**, 534–542; (*c*) A. W. Roszak, T. D. Howard, J. Southall, A. T. Gardiner, C. J. Law, N. W. Isaacs and R. J. Cogdell, *Science*, 2003, **302**, 1969–1972.
2 (*a*) S. Karrasch, P. A. Bullough and R. Ghosh, *EMBO J.*, 1995, **14**, 631–638; (*b*) S. J. Jamieson, P. Wang, P. Qian, J. Y. Kirkland, M. J. Conroy, C. N. Hunter and P. A. Bullough, *EMBO J.*, 2002, **21**, 3927–3935; (*c*) S. Scheuring, F. Francia, J. Busselez, B. A. Melandri, J.-J. Rigaud and D. Levy, *J. Biol. Chem.*, 2004, **279**, 3620–3626.
3 (*a*) S. Scheuring, J. N. Sturgis, V. Prima, A. Bernadac, D. Lévy and J.-L. Rigaud, *Proc. Natl. Acad. Sci. U. S. A.*, 2004, **101**, 11293–11297; (*b*) S. Bahatyrova, R. N. Frese, C. A. Siebert, J. D. Olsen, K. O. van der Werf, R. Van Grondelle, R. A. Niederman, P. A. Bullough, C. Otto and C. N. Hunter, *Nature*, 2004, **430**, 1058–1062; (*c*) S. Scheuring, D. Lévy and J.-L. Rigaud, *Biochim. Biophys. Acta*, 2005, **1712**, 109–127.
4 J. Pšenčík, T. P. Ikonen, P. Laurinmäki, M. C. Merckel, S. J. Butcher, R. E. Serimaa and R. Tuma, *Biophys. J.*, 2004, **87**, 1165–1172.
5 (*a*) A. Zouni, H.-T. Witt, J. Kern, P. Fromme, N. Krauß, W. Saenger and P. Orth, *Nature*, 2001, **409**, 739–744; (*b*) P. Jordan, P. Fromme, H. T. Witt, O. Klukas, W. Saenger and N. Krauß, *Nature*, 2001, **411**, 909–917.
6 (*a*) W. Kühlbrandt, D. N. Wang and Y. Fujiyoshi, *Nature*, 1994, **367**, 614–621; (*b*) Z. Liu, H. Yan, K. Wang, T. Kuang, J. Zhang, L. Gui, X. An and W. Chang, *Nature*, 2004, **428**, 287–292; (*c*) A. B. Shem, F. Frolow and N. Nelson, *Nature*, 2003, **426**, 630–635.
7 M. Kasha, H. R. Rawls and M. A. El-Bayoumi, *Pure Appl. Chem.*, 1965, **11**, 371–392.
8 (*a*) D. L. Andrews and A. A. Demidov, in *Resonance energy transfer*, Wiley, New York, 1999; (*b*) P. D. Harvey, in *The Porphyrin Handbook*, ed. K. M. Kadish, K. M. Smith and R. Guilard, Elsevier Science (USA), 2003, vol. 18, pp. 63–250.
9 M. R. Wasielewski, *Chem. Rev.*, 1992, **92**, 435–461.
10 (*a*) D. K. James and J. M. Tour, *Chem. Mater.*, 2004, **16**, 4423–4435; (*b*) E. A. Weiss, M. R. Wasielewski and M. A. Ratner, *Top. Curr. Chem.*, 2005, **257**, 103–133.
11 (*a*) H. L. Anderson, *Chem. Commun.*, 1999, 2323–2330; (*b*) O. Maury and H. L. Bozec, *Acc. Chem. Res.*, 2005, **38**, 691–704.
12 W. R. Scheidt and Y. J. Lee, *Struct. Bonding*, 1987, **64**, 1–70.
13 (*a*) P. Leighton, J. A. Cowan, R. J. Abraham and J. K. M. Sanders, *J. Org. Chem.*, 1988, **53**, 733–740. References cited in; (*b*) Y. L. Mest, M. L'Her, N. H. Hendricks, K. Kim and J. P. Collman, *Inorg. Chem.*, 1992, **31**, 835–847.
14 C. A. Hunter and J. K. M. Sanders, *J. Am. Chem. Soc.*, 1990, **112**, 5525–5534.
15 (*a*) H. Meier, Y. Kobuke and S. Kugimiya, *J. Chem. Soc., Chem. Commun.*, 1989, 923–924; (*b*) A. Osuka, S. Nakajima, T. Nagata, K. Maruyama and K. Toriumi, *Angew. Chem., Int. Ed. Engl.*, 1991, **30**, 582–584; (*c*) H. S. Cho, D. H. Jeong, M.-C. Yoon, Y. H. Kim, Y. R. Kim, D. Kim, S. C. Jeoung, S. K. Kim, N. Aratani, H. Shinmori and A. Osuka, *J. Phys. Chem. A*, 2001, **105**, 4200–4210.
16 (*a*) J. T. Fletcher and M. J. Therien, *J. Am. Chem. Soc.*, 2000, **122**, 12393–12394; (*b*) J. T. Fletcher and M. J. Therien, *J. Am. Chem. Soc.*, 2002, **124**, 4298–4311; (*c*) J. T. Fletcher and M. J. Therien, *Inorg. Chem.*, 2002, **41**, 331–341.
17 (*a*) B. Floris, M. P. Donzello and C. Ercolani, in *The Porphyrin Handbook*, ed. K. M. Kadish, K. M. Smith and R. Guilard, Elsevier Science (USA), 2003, vol. 18, pp. 1–62; (*b*) J. W. Buchler and D. K. P. Ng, in *The Porphyrin Handbook*, ed. K. M. Kadish, K. M. Smith and R. Guilard, Academic Press, San Diego, CA, 2000, vol. 3, pp. 245–294.
18 (*a*) K. Susumu, T. Shimidzu, K. Tanaka and H. Segawa, *Tetrahedron Lett.*, 1996, **37**, 8399–8402; (*b*) A. Osuka and H. Shimidzu, *Angew. Chem., Int. Ed. Engl.*, 1997, **36**, 135–137; (*c*) R. G. Khoury and L. Jaquinod, *Chem. Commun.*, 1997, **11**, 1057–1058.
19 (*a*) M. R. Wasielewski, D. G. Johnson, M. P. Niemczyk, G. L. Gaines, III, M. P. O'Neil and W. A. Svec, *J. Am. Chem. Soc.*, 1990, **112**, 6482–6488; (*b*) T. Ogawa, Y. Nishimoto, N. Yoshida, N. Ono and A. Osuka, *Angew. Chem., Int. Ed.*, 1999, **38**, 176–179.
20 (*a*) Y. F. A. Chow, D. Dolphin, J. P. Paine, III, D. McGarvey, R. Pottier and T. G. Truscott, *J. Photochem. Photobiol., B*, 1988, **2**, 253–263; (*b*) J. B. Paine, III, D. Dolphin and M. Gouterman, *Can. J. Chem.*, 1978, **56**, 1712–1715; (*c*) J. B. Paine, III and D. Dolphin, *Can. J. Chem.*, 1978, **56**, 1710–1712; (*d*) Y. Deng, C. K. Chang and D. D. Nocera, *Angew. Chem., Int. Ed.*, 2000, **39**, 1066–1068; (*e*) H. Uno, Y. Kitawaki and N. Ono, *Chem. Commun.*, 2002, **2**, 116–117; (*f*) H. Hata, H. Shinokubo and A. Osuka, *J. Am. Chem. Soc.*, 2005, **127**, 8264–8265; (*g*) T. Ikeue, K. Furukawa, H. Hata, N. Aratani, H. Shinokubo, T. Kato and A. Osuka, *Angew. Chem., Int. Ed.*, 2005, **44**, 6899–6901; (*h*) G. Bringmann, S. Ruedenauer, D. C. G. Goetz, T. A. M. Gulder and M. Reichert, *Org. Lett.*, 2006, **8**, 4743–4746.
21 (*a*) A. Tsuda, H. Furuta and A. Osuka, *Angew. Chem., Int. Ed.*, 2000, **39**, 2549–2552; (*b*) A. Tsuda and A. Osaka, *Science*, 2001, **293**, 79–82; (*c*) A. Tsuda, H. Furuta and A. Osuka, *J. Am. Chem. Soc.*, 2001, **123**, 10304–10321.
22 (*a*) V. S.-Y. Lin, S. G. DiMagno and M. J. Therien, *Science*, 1994, **264**, 1105–1111; (*b*) V. S.-Y. Lin and M. J. Therien, *Chem.–Eur. J.*, 1995, **1**, 645–651.
23 M. J. Frampton, H. Akdas, A. R. Cowley, J. E. Rogers, J. E. Slagle, P. A. Fleitz, M. Drobizhev, A. Rebane and H. L. Anderson, *Org. Lett.*, 2005, **7**, 5365–5368.
24 (*a*) D. P. Arnold, A. W. Johnson and M. Mahendran, *J. Chem. Soc., Perkin Trans. 1*, 1978, 366–370; (*b*) H. L. Anderson, *Inorg. Chem.*, 1994, **33**, 972–981.
25 D. A. Shultz, H. Lee, R. K. Kumar and K. P. Gwaltney, *J. Org. Chem.*, 1999, **64**, 9124–9136.
26 (*a*) E. M. Maya, P. Vazquez and T. Torres, *Chem. Commun.*, 1997, **13**, 1175–1176; (*b*) E. M. Maya, P. Vazquez, T. Torres, L. Gobbi, F. Diederich, S. Pyo and L. Echegoyen, *J. Org. Chem.*, 2000, **65**, 823–830.
27 S. Vigh, H. Lam, P. Janda, A. B. P. Lever, C. C. Leznoff and R. L. Cerny, *Can. J. Chem.*, 1991, **69**, 1457–1461.
28 (*a*) J. Kim and T. M. Swager, *Nature*, 2001, **411**, 1030–1034; (*b*) T. E. O. Screen, J. R. G. Thorne, R. G. Denning, D. G. Bucknall and H. L. Anderson, *J. Am. Chem. Soc.*, 2002, **124**, 9712–9713; (*c*) H. Shinmori, T. K. Ahn, H. S. Cho, D. Kim, N. Yoshida and A. Osuka, *Angew. Chem., Int. Ed.*, 2003, **42**, 2754–2758; (*d*) C. Ikeda, Z. S. Yoon, M. Park, H. Inoue, D. Kim and A. Osuka, *J. Am. Chem. Soc.*, 2005, **127**, 534–535; (*e*) A. Tsuda, H. Hu, R. Tanaka and T. Aida, *Angew. Chem., Int. Ed.*, 2005, **44**, 4884–4888.
29 Y. H. Kim, D. H. Jeong, D. Kim, S. C. Jeoung, H. S. Cho, S. K. Kim, N. Aratani and A. Osuka, *J. Am. Chem. Soc.*, 2001, **123**, 76–86.
30 K. Susumu, P. R. Frail, P. J. Angiolillo and M. J. Therien, *J. Am. Chem. Soc.*, 2006, **128**, 8380–8381.
31 M. Drobizhev, Y. Stepanenko, A. Rebane, C. J. Wilson, T. E. O. Screen and H. L. Anderson, *J. Am. Chem. Soc.*, 2006, **128**, 12432–12433.
32 (*a*) J. M. Tour, *Chem. Rev.*, 1996, **96**, 537–553; (*b*) T. Aida and D.-L. Jiang, in *The Porphyrin Handbook*, ed. K. M. Kadish, K. M. Smith and R. Guilard, Academic Press, San Diego, CA, 2000, vol. 3, pp. 369–384; (*c*) V. Balzani, P. Ceroni, A. Juris, M. Venturi, S. Campagna, F. Puntoriero and S. Serroni, *Coord. Chem. Rev.*, 2001, **219**, 545–572; (*d*) H. Imahori, *J. Phys. Chem. B*, 2004, **108**, 6130–6143.
33 (*a*) M.-S. Choi, T. Aida, T. Yamazaki and I. Yamazaki, *Angew. Chem., Int. Ed.*, 2001, **40**, 3194–3198; (*b*) E. K. L. Yeow, K. P. Ghiggino, J. N. H. Reek, M. J. Crossley, A. W. Bosman, A. P. H. J. Schenning and E. W. Meijer, *J. Phys. Chem. B*, 2000, **104**, 2596–2606; (*c*) W.-S. Li, K. S. Kim,

D.-L. Jiang, H. Tanaka, T. Kawai, J. H. Kwon, D. Kim and T. Aida, *J. Am. Chem. Soc.*, 2006, **128**, 10527–10532.
34 J. W. Steed and J. L. Atwood, *Supramolecular Chemistry*, Wiley & Sons, Chichester, 2000.
35 (*a*) A. Satake and Y. Kobuke, *Tetrahedron*, 2005, **61**, 13–41; (*b*) Y. Kobuke, *Struct. Bonding*, 2006, **121**, 49–104.
36 R. T. Stibrany, J. Vasudevan, S. Knapp, J. A. Potenza, T. Emge and H. J. Schugar, *J. Am. Chem. Soc.*, 1996, **118**, 3980–3981.
37 Y. Kobuke and H. Miyaji, *J. Am. Chem. Soc.*, 1994, **116**, 4111–4112.
38 C. Ikeda, Y. Tanaka, T. Fujihara, Y. Ishii, T. Ushiyama, K. Yamamoto, N. Yoshioka and H. Inoue, *Inorg. Chem.*, 2001, **40**, 3395–3405.
39 (*a*) M. Gardner, A. J. Guerin, C. A. Hunter, U. Michelsen and C. Rotger, *New J. Chem.*, 1999, **23**, 309–316; (*b*) S. Knapp, J. Vasudevan, T. J. Emge, B. H. Arison, J. A. Potenza and H. J. Schugar, *Angew. Chem., Int. Ed.*, 1998, **37**, 2368–2370.
40 T. H. Tran Thi, C. Desforge, C. Thiec and S. Gaspard, *J. Phys. Chem.*, 1989, **93**, 1226–1233.
41 N. Kobayashi and A. B. P. Lever, *J. Am. Chem. Soc.*, 1987, **109**, 7433–7441.
42 (*a*) J. P. Fillers, K. G. Ravichandran, I. Abdalmuhdi, A. Tulinsky and C. K. Chang, *J. Am. Chem. Soc.*, 1986, **108**, 417–424; (*b*) F. Bolze, C. P. Gros, M. Drouin, E. Espinosa, P. D. Harvey and R. Guilard, *J. Organomet. Chem.*, 2002, **643–644**, 89–97; (*c*) S. Faure, C. Stern, R. Guilard and P. D. Harvey, *J. Am. Chem. Soc.*, 2004, **126**, 1253–1261; (*d*) Y. Deng, C. J. Chang and D. G. Nocera, *J. Am. Chem. Soc.*, 2000, **122**, 410–411.
43 A. Osuka and K. Maruyama, *J. Am. Chem. Soc.*, 1988, **110**, 4454–4456.
44 Y. Kobuke and K. Ogawa, *Bull. Chem. Soc. Jpn.*, 2003, **76**, 689–708.
45 A. Satake, O. Shoji and Y. Kobuke, *J. Organomet. Chem.*, 2007, **692**, 635–644.
46 The orientation factors and distances were estimated from molecular models constructed by Material Studio® with a semi-empirical MO calculation (AM1).
47 D. Furutsu, A. Satake and Y. Kobuke, *Inorg. Chem.*, 2005, **44**, 4460–4462.
48 L. Oddos-Marcel, F. Madeore, A. Bock, D. Neher, A. Ferencz, H. Rengel, G. Wegner, C. Kryschi and H. P. Trommsdorff, *J. Phys. Chem.*, 1996, **100**, 11850–11856.
49 U. Rösch, S. Yao, R. Wortmann and F. Würthner, *Angew. Chem., Int. Ed.*, 2006, **45**, 7026–7030.
50 C. Galli, K. Wynne, S. M. LeCours, M. J. Therien and R. M. Hochstrasser, *Chem. Phys. Lett.*, 1993, **206**, 493–499.
51 W.-S. Li, D.-L. Jiang and T. Aida, *Angew. Chem., Int. Ed.*, 2004, **43**, 2943–2947.
52 D. Kalita, M. Morisue and Y. Kobuke, *New J. Chem.*, 2006, **30**, 77–92.
53 F. Hajjaj, Z. S. Yoon, M. Yoon, J. Park, A. Satake, D. Kim and Y. Kobuke, *J. Am. Chem. Soc.*, 2006, **128**, 4612–4623.
54 J. Tanihara, K. Ogawa and Y. Kobuke, *J. Photochem. Photobiol., A*, 2006, **178**, 140–149.
55 K. Ogawa and Y. Kobuke, *Angew. Chem., Int. Ed.*, 2000, **39**, 4070–4073.
56 (*a*) R. Takahashi and Y. Kobuke, *J. Am. Chem. Soc.*, 2003, **125**, 2372–2373; (*b*) C. Ikeda, A. Satake and Y. Kobuke, *Org. Lett.*, 2003, **5**, 4935–4938; (*c*) R. Takahashi and Y. Kobuke, *J. Org. Chem.*, 2005, **70**, 2745–2753.
57 A. Ohashi, A. Satake and Y. Kobuke, *Bull. Chem. Soc. Jpn.*, 2004, **77**, 365–374.
58 I.-W. Hwang, M. Park, T. K. Ahn, Z. S. Yoon, D. M. Ko, D. Kim, F. Ito, Y. Ishibashi, S. R. Khan, Y. Nagasawa, H. Miyasaka, C. Ikeda, R. Takahashi, K. Ogawa, A. Satake and Y. Kobuke, *Chem.–Eur. J.*, 2005, **11**, 3753–3761.
59 I.-W. Hwang, T. Kamada, T. K. Ahn, D. M. Ko, T. Nakamura, A. Tsuda, A. Osuka and D. Kim, *J. Am. Chem. Soc.*, 2004, **126**, 16187–16198.
60 S. E. Bradforth, R. Jimenez, F. van Mourik, R. van Grondelle and G. R. Fleming, *J. Phys. Chem.*, 1995, **99**, 16179–16191.
61 A. Satake, H. Tanaka, F. Hajjaj, T. Kawai and Y. Kobuke, *Chem. Commun.*, 2006, 2542–2544.
62 Y. Kuramochi, A. Satake and Y. Kobuke, *J. Am. Chem. Soc.*, 2004, **126**, 8668–8669.
63 O. Shoji, S. Okada, A. Satake and Y. Kobuke, *J. Am. Chem. Soc.*, 2005, **127**, 2201–2210.
64 O. Shoji, H. Tanaka, T. Kawai and Y. Kobuke, *J. Am. Chem. Soc.*, 2005, **127**, 8598–8599.
65 (*a*) X. Peng, N. Aratani, A. Takagi, T. Matsumoto, T. Kawai, I.-W. Hwang, T. K. Ahn, D. Kim and A. Osuka, *J. Am. Chem. Soc.*, 2004, **126**, 4468–4469; (*b*) I.-W. Hwang, D. M. Ko, T. K. Ahn, Z. S. Yoon, D. Kim, X. Peng, N. Aratani and A. Osuka, *J. Phys. Chem. B*, 2005, **109**, 8643–8651.
66 T. Hori, N. Aratani, A. Takagi, T. Matsumoto, T. Kawai, M.-C. Yoon, Z. S. Yoon, S. Cho, D. Kim and A. Osuka, *Chem.–Eur. J.*, 2006, **12**, 1319–1327.
67 (*a*) R. A. Haycock, C. A. Hunter, D. A. James, U. Michelsen and L. R. Sutton, *Org. Lett.*, 2000, **2**, 2435–2438; (*b*) C. Ikeda, E. Fujiwara, A. Satake and Y. Kobuke, *Chem. Commun.*, 2003, 616–617.
68 Y. Inaba and Y. Kobuke, *Tetrahedron*, 2004, **60**, 3097–3107.
69 (*a*) T. Miyatake and H. Tamiaki, *J. Photochem. Photobiol., C*, 2005, **6**, 89–107; (*b*) T. S. Balaban, *Acc. Chem. Res.*, 2005, **38**, 612–623.
70 J. Vasudevan, R. T. Stibrany, J. Bumby, S. Knapp, J. A. Potenza, T. J. Emge and H. J. Schugar, *J. Am. Chem. Soc.*, 1996, **118**, 11676–11677.
71 K. Kameyama, M. Morisue, A. Satake and Y. Kobuke, *Angew. Chem., Int. Ed.*, 2005, **44**, 4763–4766.
72 (*a*) N. Kobayashi, *Coord. Chem. Rev.*, 2002, **227**, 129–152; (*b*) A. W. Snow, in *The Porphyrin Handbook*, ed. K. M. Kadish, K. M. Smith and R. Guilard, Elsevier Science, USA, 2003, vol. 17, pp. 129–176; (*c*) M. J. Cook and I. Chambrier, in *The Porphyrin Handbook*, ed. K. M. Kadish, K. M. Smith and R. Guilard, Elsevier Science, USA, 2003, vol. 17, pp. 37–127; (*d*) D. Dini and M. Hanack, in *The Porphyrin Handbook*, ed. K. M. Kadish, K. M. Smith and R. Guilard, Elsevier Science, USA, 2003, vol. 17, pp. 1–36; (*e*) M. K. Engel, in *The Porphyrin Handbook*, ed.K. M. Kadish, K. M. Smith and R. Guilard, Elsevier Science, USA, 2003, vol. 20, pp. 1–242.
73 H. Lam, S. M. Marcuccio, P. I. Svirskaya, S. Greenberg, A. B. P. Lever, C. C. Leznoff and R. L. Cerny, *Can. J. Chem.*, 1989, **67**, 1087–1097.
74 (*a*) A. Escosura, M. V. Martínez-Díaz, P. Thordarson, A. E. Rowan, R. J. M. Nolte and T. Torres, *J. Am. Chem. Soc.*, 2003, **125**, 12300–12308; (*b*) Y. Asano, A. Muranaka, A. Fukasawa, T. Hatano, M. Uchiyama and N. Kobayashi, *J. Am. Chem. Soc.*, 2007, **129**, 4516–4517.
75 N. Kobayashi, T. Fukuda and D. Lelièvre, *Inorg. Chem.*, 2000, **39**, 3632–3637.
76 K. Ishii and N. Kobayashi, in *The Porphyrin Handbook*, ed. K. M. Kadish, K. M. Smith and R. Guilard, Elsevier Science, USA, 2003, vol. 16, pp. 1–42.
77 T.-H. Tran-Thi, *Coord. Chem. Rev.*, 1997, **160**, 53–91.
78 K. Kameyama, A. Satake and Y. Kobuke, *Tetrahedron Lett.*, 2004, **45**, 7617–7620.
79 J. P. C. Tomé, A. M. V. M. Pereira, C. M. A. Alonso, M. G. P. M. S. Neves, A. C. Tomé, A. M. S. Silva, J. A. S. Cavaleiro, M. V. Martínez-Díaz, T. Torres, G. M. A. Rahman, J. Ramey and D. M. Guldi, *Eur. J. Org. Chem.*, 2006, 257–267.
80 F. Ito, Y. Ishibashi, S. R. Khan, H. Miyasaka, K. Kameyama, M. Morisue, A. Satake, K. Ogawa and Y. Kobuke, *J. Phys. Chem. A*, 2006, **110**, 12734–12742.
81 H. Ozeki, A. Nomoto, K. Ogawa, Y. Kobuke, M. Murakami, K. Hosoda, M. Ohtani, S. Nakashima, H. Miyasaka and T. Okada, *Chem.–Eur. J.*, 2004, **10**, 6393–6401.
82 (*a*) A. Nomoto and Y. Kobuke, *Chem. Commun.*, 2002, 1104–1105; (*b*) M. Morisue, S. Yamatsu, N. Haruta and Y. Kobuke, *Chem.–Eur. J.*, 2005, **11**, 5563–5574.